

PRIMUS: OBSCURED STAR FORMATION ON THE RED SEQUENCE

GUANGTUN ZHU¹, MICHAEL R. BLANTON¹, SCOTT M. BURLLES², ALISON L. COIL^{3,7}, RICHARD J. COOL^{4,8}, DANIEL J. EISENSTEIN⁵, JOHN MOUSTAKAS³, KENNETH C. WONG⁶, AND JAMES AIRD³

ACCEPTED FOR PUBLICATION IN THE ASTROPHYSICAL JOURNAL: November 8, 2010

ABSTRACT

We quantify the fraction of galaxies at moderate redshifts ($0.1 < z < 0.5$) that appear red-and-dead in the optical, but in fact contain obscured star formation detectable in the infrared (IR), with the PRIMUS Multi-object Survey (PRIMUS). PRIMUS has measured $\sim 120,000$ robust redshifts with a precision of $\sigma_z/(1+z) \sim 0.5\%$ over 9.1 deg^2 of the sky to the depth of $i \sim 23$ (AB), up to redshift $z \sim 1$. We specifically targeted 6.7 deg^2 fields with existing deep IR imaging from the *Spitzer Space Telescope* from the SWIRE and S-COSMOS surveys. We select in these fields an i band flux-limited sample ($i < 20$ mag in the SWIRE fields and $i < 21$ mag in the S-COSMOS field) of 3310 red-sequence galaxies at $0.1 < z < 0.5$ for which we can reliably classify obscured star-forming and quiescent galaxies using IR color. Our sample constitutes the largest galaxy sample at intermediate redshift to study obscured star formation on the red sequence, and we present the first quantitative analysis of the fraction of obscured star-forming galaxies as a function of luminosity. We find that on average, at $L \sim L^*$, about 15% of red-sequence galaxies have IR colors consistent with star-forming galaxies. The percentage of obscured star-forming galaxies increases by $\sim 8\%$ per mag with decreasing luminosity from the highest luminosities to $L \sim 0.2L^*$. Our results suggest that a significant fraction of red-sequence galaxies have ongoing star formation and that galaxy evolution studies based on optical color therefore need to account for this complication.

Subject headings: galaxies: fundamental parameters (classification, colors, luminosities, masses, radii, etc.) — galaxies: distances and redshifts — galaxies: evolution — stars: formation — dust, extinction

1. INTRODUCTION

Our understanding of the formation and evolution of galaxies has improved tremendously the last few decades as a result of multiple redshift surveys (e.g., Davis et al. 1982; York et al. 2000; Colless et al. 2001; Wolf et al. 2003; Davis et al. 2003; Lilly et al. 2007; Garilli et al. 2008). These surveys have demonstrated that the distribution of galaxy populations is bimodal in the optical color-magnitude space up to $z \sim 2.5$ (e.g., Strateva et al. 2001; Blanton et al. 2003a; Baldry et al. 2004; Balogh et al. 2004; Bell et al. 2004b; Willmer et al. 2006; Wuyts et al. 2007; Williams et al. 2009; Brammer et al. 2009, among others). The underlying physical reason is the short lifetime of massive stars. Once star formation stops in a galaxy, hot massive stars quickly die, the integrated spectral energy distribution (SED) of the galaxy becomes dominated by cool giants, and its optical color turns from blue to red. The bimodal-

ity of blue cloud and red sequence in the color-magnitude diagram therefore approximately translates into that of star-forming (SF) and quiescent galaxies.

Recent studies of the mass and luminosity functions of red-sequence galaxies at different redshifts show that the stellar mass density on the red sequence has increased by a factor of ~ 2 overall since $z \sim 1$ (e.g., Bell et al. 2004b; Faber et al. 2007). This build-up could result from some combination of migration from the blue cloud (due to mergers, feedback or other mechanisms for turning off star formation) and gas-poor, “dry” merging from smaller-mass red-sequence galaxies (e.g., Bell et al. 2004b, 2006a,b). Other studies (e.g., Cimatti et al. 2006; Brown et al. 2007; Cool et al. 2008) find that the growth of the red-sequence populations depends strongly on luminosity: whereas many L^* red-sequence galaxies assembled in the time since $z \sim 1$, at the massive end ($L \gtrsim 3L^*$) the mass and luminosity functions are consistent with passive evolution. They therefore argue that merging (dry or wet) does not dominate the evolution of massive red galaxies since $z \sim 1$.

One complication that current studies of red-sequence galaxies ignore is that optically red galaxies can have *in situ*, but dust-obscured star formation. Because of this dust-obscuration, optical color can be a misleading proxy for star formation. Dust extinction reshapes the SED of a galaxy, absorbing photons at high energy (e.g., ultraviolet, UV) and re-emitting the energy at longer wavelengths (e.g., infrared, IR). Therefore the red sequence consists of both truly quiescent but also obscured SF galaxies; it is extremely important to quantify the composition of the red sequence to obtain an accurate un-

¹ Center for Cosmology and Particle Physics, Department of Physics, New York University, 4 Washington Place, New York, NY 10003; gz323@nyu.edu

² D.E. Shaw & Co., L.P., 20400 Stevens Creek Blvd., Suite 850, Cupertino, CA 95014

³ Department of Physics, Center for Astrophysics and Space Sciences, University of California, 9500 Gilman Dr., La Jolla, San Diego, CA 92093

⁴ Department of Astrophysical Sciences, Princeton University, Peyton Hall, Princeton, NJ 08544

⁵ Department of Astronomy, Harvard University, 60 Garden Street, Cambridge, MA 02138

⁶ Steward Observatory, University of Arizona, 933 North Cherry Avenue, Tucson, AZ 85721

⁷ Alfred P. Sloan Foundation Fellow

⁸ Hubble Fellow and Carnegie-Princeton Fellow

derstanding of galaxy evolution.

There are several ways to investigate the contribution of obscured SF galaxies on the red sequence. Assuming inclination is well-correlated with dust extinction along the line-of-sight, Maller et al. (2009, see also Shao et al. 2007; Unterborn & Ryden 2008; Bailin & Harris 2008b) find the ratio of red-to-blue galaxies changes from 1:1 to 1:2 when moving from observed to inclination-corrected color, for local galaxies in the Sloan Digital Sky Survey (SDSS, York et al. 2000). Using deep imaging from the *Hubble Space Telescope* (*HST*) from the Galaxy Evolution from Morphology and SED project (GEMS, Rix et al. 2004) and photometric redshifts from the COMBO-17 survey (Wolf et al. 2003), Bell et al. (2004a) find that less than 13% of red-sequence galaxies are edge-on dusty disk galaxies at $z \sim 0.7$. One can also correct dust extinction by fitting multi-wavelength data or SEDs with stellar population synthesis models and allowing dust extinction to be a free parameter. Using this method on COMBO-17 data, Wolf et al. (2005) find a rich component of dusty SF galaxies contaminating the red sequence in the cluster Abell 901/902 at $z \sim 0.17$. The mid-IR (MIR) emission from dust offers another method for selecting obscured SF galaxies, though the emission can also originate from strong active galactic nuclei (AGNs). Brand et al. (2009, see also Coia et al. 2005; Davoodi et al. 2006; Rodighiero et al. 2007; Saintonge et al. 2008) discover $\sim 10\%$ of red-sequence galaxies at $0.15 \leq z \leq 0.3$ exhibit strong MIR 24 μm emission with $f_{24} > 300 \mu\text{Jy}$. We can also use IR color to separate SF and quiescent galaxies. At wavelengths $< 10 \mu\text{m}$, warm dust emission and strong polycyclic aromatic hydrocarbon (PAH) features dominate the SED of SF galaxies, producing much redder IR colors than expected from quiescent galaxies. Brand et al. (2009) use this method and find that, among the $\sim 10\%$ of red-sequence galaxies with $f_{24} > 300 \mu\text{Jy}$ in their sample, about 64% have IR colors consistent with SF galaxies, with the rest consistent with quiescent galaxies (31%) and AGNs (5%).

Quantitative studies of obscured star formation at intermediate and high redshifts are usually limited to small samples. For example, Wolf et al. (2005) select 462 red-sequence galaxies in a specific environment, the Abell 901/902 super-cluster system. Even though deep multi-wavelength data including space-based IR imaging are now available across a large area of the sky, the lack of corresponding large redshift surveys hampers the systematic quantitative studies of the contribution of obscured SF galaxies on the red sequence. We have recently completed such a redshift survey, the PRISM MUlti-object Survey (PRIMUS⁹), to provide the redshifts required to fully realize the science potential of the existing deep multi-wavelength imaging data.

PRIMUS has measured $\sim 120,000$ robust redshifts over 9.1 deg^2 of the sky to the depth of $i \sim 23$ (AB) up to redshift $z \sim 1$. We specifically targeted areas where there exist deep multi-wavelength imaging data, including IR data from the *Spitzer Space Telescope* (Werner et al. 2004), making our dataset ideal for the study of the obscured star formation on the red sequence. Using the IR data, in conjunction with the redshifts from PRIMUS,

we here present the first quantitative study of the fraction of obscured SF galaxies on the red sequence as a function of luminosity at redshifts $0.1 < z < 0.5$.

This paper proceeds as follows. In Section 2, we briefly introduce PRIMUS and describe the *Spitzer* data we use. In Section 3, we describe in detail the classification scheme for AGNs, star-forming galaxies, and quiescent galaxies. We present the results in Section 4. In Section 5, we discuss the composition of the red sequence. We summarize our principal conclusions in Section 6.

Throughout this work, we adopt a Λ CDM cosmological model with $\Omega_m = 0.3$, $\Omega_\Lambda = 0.7$ and $H_0 = 100h \text{ km s}^{-1} \text{ Mpc}^{-1}$. If not specifically mentioned, all magnitudes are on the AB system.

2. DATA

2.1. PRIMUS

PRIMUS is a unique low-resolution spectroscopic intermediate redshift survey. We conducted the survey using the IMACS instrument on the Magellan I (Baade) Telescope at Las Campanas Observatory. With a prism and slitmasks, we obtained low-resolution spectra for $\sim 300,000$ objects to the depth of $i \sim 23$ out to redshift $z \sim 1$ in 39 nights, covering 9.1 deg^2 of the sky. The low-resolution of the prism ($R \sim 30 - 150$) allows us to observe ~ 2500 objects in one single mask with a field of view 0.18 deg^2 . By carefully fitting the low-resolution spectra with galaxy spectral templates, we have obtained $\sim 120,000$ robust redshifts, to the precision of $\sigma_z/(1+z) \sim 0.5\%$. PRIMUS therefore is the largest faint galaxy redshift survey performed to date.

When designing the survey, we specifically targeted fields with existing deep multi-wavelength imaging, including optical imaging from various ground-based deep surveys, near-UV (NUV) and far-UV (FUV) from the Galaxy Evolution Explorer (*GALEX*, Martin et al. 2005), IR from the *Spitzer Space Telescope*, and X-ray from *Chandra* and/or *XMM* telescopes.

We created homogeneous band-merged catalogs across all our fields. With the redshifts and the band-merged catalogs, we derived absolute magnitudes using the `kcorrect` package (v4.1.4 Blanton & Roweis 2007). Because we focus on redshifts $0.1 < z < 0.5$, here we use the absolute magnitudes at *ugriz* bands shifted blueward to $z = 0.3$ (e.g., Blanton et al. 2003a). We denote these bands with a preceding superscript 0.3, e.g., $^{0.3}i$. For a galaxy exactly at redshift 0.3 with apparent magnitude i , the K -correction from i to $M_{0.3i}$ is simply $-2.5 \log_{10}(1+z)$ independent of galaxy SED. This filter choice therefore minimizes the error in the K -corrections.

When fitting for the redshift, we also fit the spectra with stellar and broad-line AGN spectral templates and classify objects into stars, AGNs, and galaxies based upon the χ^2 of the best fits. In $\sim 5.5 \text{ deg}^2$ of the 9.1 deg^2 PRIMUS fields, we have X-ray data from *Chandra* and/or *XMM* telescopes. Here we select our sample only from objects that are classified as galaxies and do not have matched X-ray detections.

For more details on the PRIMUS survey, we refer the reader to the survey papers (Coil et al. 2010, Cool et al., in prep.).

2.2. *Spitzer Space Telescope*

⁹ <http://cass.ucsd.edu/~acoil/primus/>

In $\sim 7.2 \text{ deg}^2$ of the 9.1 deg^2 fields covered by PRIMUS we have IR imaging data from The Infrared Array Camera (IRAC, Fazio et al. 2004) and The Multi-band Imaging Photometer (MIPS, Rieke et al. 2004) onboard *Spitzer*. IRAC is a four-channel instrument that provides simultaneous broadband images at 3.6 , 4.5 , 5.8 and $8.0 \mu\text{m}$ with unprecedented sensitivity. MIPS provides images at longer wavelengths, 24 , 70 and $160 \mu\text{m}$ with 5σ rms depths of 0.3 mJy , 25 mJy and 150 mJy , respectively. Here we use the $\sim 6.7 \text{ deg}^2$ that has coverage from all four channels of IRAC and $24 \mu\text{m}$ band of MIPS. For $\sim 0.5 \text{ deg}^2$ of the DEEP2 (Davis et al. 2003) field with the IRAC imaging, only the $3.6 \mu\text{m}$ and $4.5 \mu\text{m}$ imaging is available; we omit this field, because we require all four channels for this paper. The data we use consist of two Legacy Programs of *Spitzer*, 5.7 deg^2 in three fields of *Spitzer* Wide-area Infrared Extragalactic Survey (SWIRE¹⁰; Lonsdale et al. 2003), and 1 deg^2 in the *Spitzer* Deep Survey of the *HST* COSMOS 2-Degree ACS Field (S-COSMOS¹¹; Sanders et al. 2007). We use the data release 2 and 3 of the SWIRE survey, and the public catalog in the NASA/IPAC Infrared Science Archive for the S-COSMOS survey. In most of the SWIRE fields, to at least 5σ depths, the flux limits in the four IRAC channels are 10 , 10 , 43 , and $40 \mu\text{Jy}$ (21.4 , 21.4 , 19.8 and 19.9 AB mag^{12}). The flux limits in the S-COSMOS field are 0.9 , 1.7 , 11.3 , and $14.6 \mu\text{Jy}$ (24.0 , 23.3 , 21.3 and 21.0 AB mag), in the four IRAC channels, respectively.

At wavelengths $< 10 \mu\text{m}$, warm dust emission and strong PAH features, e.g. 3.3 , 6.2 , 7.7 and $8.6 \mu\text{m}$, dominate the SED of a typical SF galaxy (Li & Draine 2001; Smith et al. 2007). Moving to higher redshift, the 6.2 , 7.7 and $8.6 \mu\text{m}$ PAH emission bands shift through the IRAC $8.0 \mu\text{m}$ channel, producing much redder IRAC colors than expected from a typical quiescent early-type galaxy. Red-sequence galaxies whose star formation is obscured by dust have IRAC colors consistent with normal SF galaxies. Strong AGNs, on the other hand, occupy a different locus from regular SF and quiescent galaxies in the IRAC color-color diagram (Eisenhardt et al. 2004; Lacy et al. 2004; Stern et al. 2005). The IRAC colors therefore are extremely convenient and powerful for classification of AGNs, SF galaxies, and quiescent galaxies. We discuss this in detail in Section 3.

3. SOURCE SELECTION

3.1. Flux-limited sample in i band

In order to use IR color to identify SF galaxies, we restrict our sample to the PRIMUS fields with IR coverage (6.7 deg^2). We also only select our sample from galaxies with the highest confidence ($\mathbf{Q} = 4$, see Cool et al. in prep. for details on the confidence level \mathbf{Q}).

We also need to select appropriate flux limits in the i band and the $3.6 \mu\text{m}$ band, which are necessarily related to the depth of the coverage in the $8.0 \mu\text{m}$ band. The

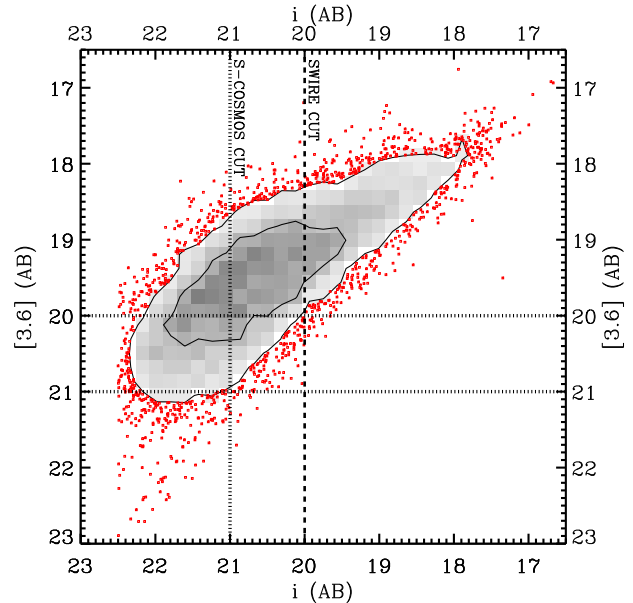


FIG. 1.— Selection of the i band flux-limited sample. We present $[3.6]$ vs. i for red-sequence galaxies. The detection limits in the $8.0 \mu\text{m}$ channel are 19.9 (21.0) mag in the SWIRE (S-COSMOS) fields, effectively much brighter than the limits in the $3.6 \mu\text{m}$ channel. Many $3.6 \mu\text{m}$ detections are not detected in the $8.0 \mu\text{m}$ channel. We can only use the IR color $[3.6] - [8.0]$ to perform reliable star-forming and quiescent galaxy classification for objects with bright $3.6 \mu\text{m}$ fluxes with $[3.6] \lesssim 20$ (21) mag. We show here that most of the red-sequence galaxies with $i < 20$ (21) mag have $[3.6] < 20$ (21) mag. We therefore only select galaxies with i brighter than 20 (21) mag in the SWIRE (S-COSMOS) fields. In Section 3.4, we show that these cuts enable us to classify almost all non-detections in $8.0 \mu\text{m}$ channel as quiescent galaxies in this flux-limited red-sequence sample.

flux limits used in the $8.0 \mu\text{m}$ channel are 19.9 mag in the SWIRE fields and 21.0 mag in the S-COSMOS field, effectively much brighter than those in the $3.6 \mu\text{m}$ channel (21.4 and 24.0 mag). Thus, in order to place interesting limits on the specific star-formation rate (SSFR) using the $[3.6] - [8.0]$ color, we must restrict our sample to bright enough galaxies. In Section 3.4, we will show that galaxies with SSFR of $\sim 10^{-10} \text{ yr}^{-1}$ have colors $[3.6] - [8.0] \gtrsim 0$ and quiescent galaxies have $[3.6] - [8.0] \lesssim 0$. Our definition of “star-forming” will be loosely related to this SSFR, and this color cut defines how bright our sample needs to be. We thus require the upper limits of the $[3.6] - [8.0]$ colors of the $8.0 \mu\text{m}$ non-detections to be $\lesssim 0$ so that we can reliably classify them into quiescent galaxies, or in other words that the $[3.6]$ magnitudes should be brighter than ~ 20 (21) mag in the SWIRE (S-COSMOS) fields.

We achieve this by applying appropriate limits in the i band. In Figure 1, we present the $[3.6]$ versus i for the red-sequence galaxies (defined in the next section), where we have shown $[3.6] = 20$ and 21 mag with two horizontal lines. We see that for most of the red-sequence galaxies with $i < 20$ (21) mag, they have $3.6 \mu\text{m}$ magnitudes $[3.6] < 20$ (21). We therefore define a flux-limited sample with $i < 20$ and $i < 21$, in the SWIRE and S-COSMOS fields, respectively. We will further justify these cuts in Section 3.4, where we explicitly demonstrate that after these cuts, virtually all $8.0 \mu\text{m}$ non-detections are quies-

¹⁰ <http://swire.ipac.caltech.edu/swire/swire.html>

¹¹ <http://irsa.ipac.caltech.edu/data/SPITZER/S-COSMOS/>; COSMOS represents the Cosmological Evolution Survey and ACS is the Advanced Camera for Surveys onboard *HST*.

¹² We use AB magnitudes throughout this work but also give Vega magnitudes when necessary. The conversion factors (AB–Vega) for IRAC 3.6 , 4.5 , 5.8 , and $8.0 \mu\text{m}$ are 2.79 , 3.26 , 3.73 , and 4.40 mag, respectively.

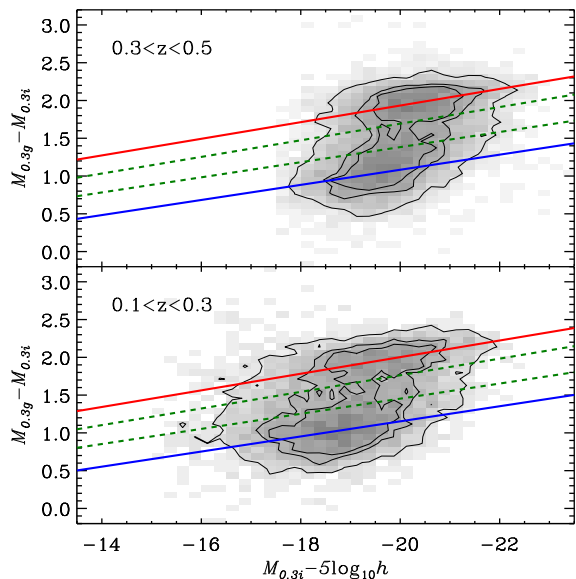


FIG. 2.— Color-magnitude diagram of galaxies with $i < 22.5$. We use the absolute magnitudes in g and i bands shifted blueward to $z = 0.3$ ($^{0.3}g$ and $^{0.3}i$) to minimize the errors in K -corrections. We show the diagram in two redshift bins: $0.1 < z < 0.3$ (lower panel) and $0.3 < z < 0.5$ (upper panel). The red solid lines and the blue solid lines indicate the positions of the red sequence and the blue cloud. The two green dashed lines represent the selection criteria (Equation (1) and (2)) we adopt to select red-sequence and blue-cloud galaxies, at median redshift in each bin. Galaxies between them are identified as green-valley galaxies. At different redshifts, we fix the slope of the criteria but allow the intercept to evolve (redder) by 0.4 per unit redshift.

cent galaxies.

Beyond redshift 0.5, the $6.2 \mu\text{m}$ PAH feature shifts out of the $8.0 \mu\text{m}$ channel and we can not use the $[3.6] - [8.0]$ color to reliably separate SF and quiescent galaxies. We also do not have many galaxies below redshift 0.1 in the PRIMUS fields due to the small volume. Therefore, we focus our analysis on the redshift range $0.1 < z < 0.5$. We will come back to this in Section 3.4. In total, the flux-limited sample within $0.1 < z < 0.5$ includes 7258 galaxies.

3.2. Red sequence, blue cloud, and green valley

To define the red sequence, blue cloud, and green valley, we use all galaxies with $i < 22.5$ with secure redshifts ($Q = 4$) in PRIMUS. PRIMUS targeted in i band unless there is no i band imaging available, in which case we used R band. We thus choose to use the magnitude $M_{0.3i} - 5 \log_{10} h$, and the color $M_{0.3g} - M_{0.3i}$ when defining samples based on optical color. At each luminosity, we fit the color distribution with a two-gaussian model. We then linearly fit the two sets of peaks to obtain the slopes and intercepts of the red sequence and the blue cloud. To define the edges of green valley, we move the fitted line for the red sequence (blue cloud) blueward (redward) until it includes 60% more galaxies above (below) the line. This method allows us to conservatively select red-sequence and blue-cloud galaxies, without contamination from green-valley galaxies. Due to passive evolution, the colors of galaxies at lower redshift are redder than those at higher redshift. Therefore, we keep

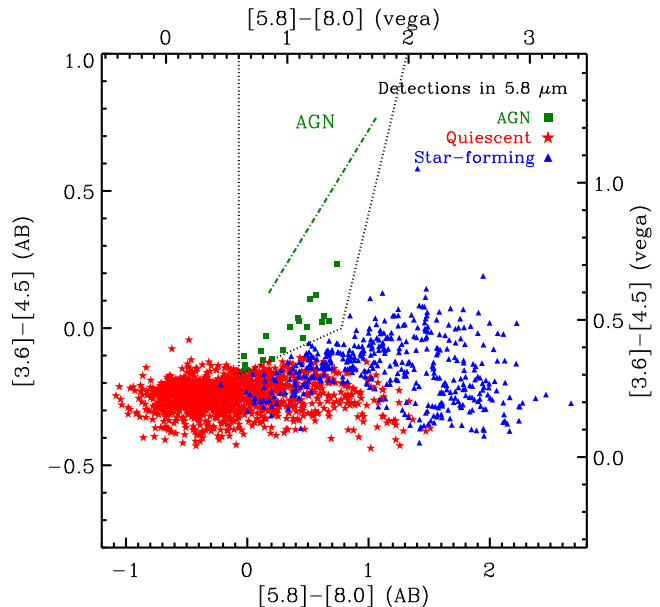


FIG. 3.— AGN classification for detections in both the $5.8 \mu\text{m}$ and the $8.0 \mu\text{m}$ channels in the flux-limited red-sequence sample. We show the IRAC color-color diagram with $[3.6] - [4.5]$ vs. $[5.8] - [8.0]$. The dotted wedge shows the criteria for AGN selection suggested by Stern et al. (2005). The dot-dashed line represents the colors of power-law spectra $f(\nu) = \nu^{-\alpha}$ of AGNs with the index α ranging from 0.5 to 3.0. Galaxies that fall into the wedge are identified as AGNs. For non-AGN galaxies, we use the $[3.6] - [8.0]$ color to classify them into star-forming galaxies and quiescent galaxies (Section 3.4). We show the SF galaxies in blue filled triangles and the quiescent galaxies in red filled stars.

the slope fixed throughout the redshift range, but allow the intercept to evolve linearly in redshift. By fitting the color-magnitude diagram at different redshifts, we measure the color reddening is ~ 0.4 per unit redshift in $M_{0.3g} - M_{0.3i}$.

Finally, the criteria we adopt are as follows. We require a red-sequence galaxy to have the color:

$$M_{0.3g} - M_{0.3i} > 1.73 - 0.11(M_{0.3i} - 5 \log_{10} h + 20) - 0.4(z - 0.3), \quad (1)$$

and a blue-cloud galaxy to have the color:

$$M_{0.3g} - M_{0.3i} < 1.40 - 0.10(M_{0.3i} - 5 \log_{10} h + 20) - 0.4(z - 0.3). \quad (2)$$

Between these two criteria, we identify objects as green-valley galaxies. As an example, in Figure 2, we show the color-magnitude diagram of all galaxies with $i < 22.5$ at $0.3 < z < 0.5$ (upper panel) and at $0.1 < z < 0.3$ (lower panel). The two solid lines in each panel represent the positions of the red sequence and the blue cloud, and the dashed lines indicate the edges of the green valley, i.e., the criteria defined by Equation (1) and (2) at median redshift in each bin.

Finally, in the flux-limited sample, we have 3310 red-sequence galaxies, 2497 blue-cloud galaxies and 1451 green-valley galaxies.

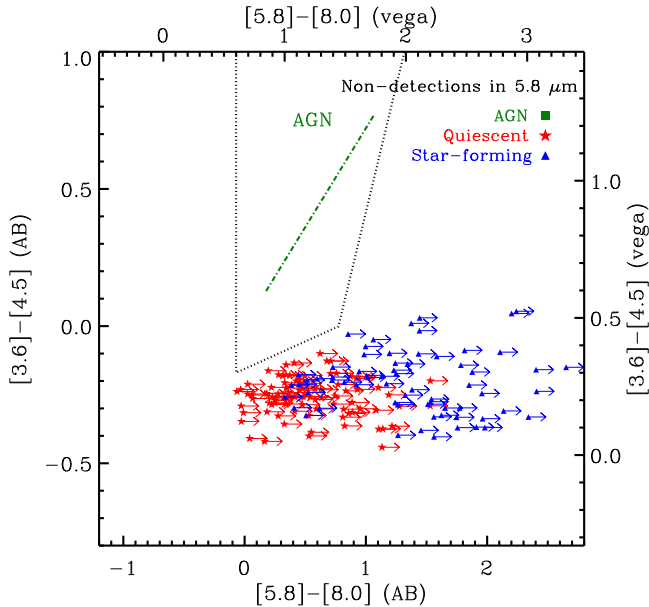


FIG. 4.— AGN classification for non-detections in the $5.8 \mu\text{m}$ channel that are detected in the $8.0 \mu\text{m}$ channel in the flux-limited red-sequence sample. We use the flux limits of $[5.8] < 19.8$ (21.0) mag in the SWIRE (S-COSMOS) fields to calculate the lower limits of their $[5.8] - [8.0]$ colors. We can safely treat all the non-detections as non-AGNs.

3.3. AGN identification

For the purposes of this paper, we are primarily interested in star-forming galaxies, and attempt to identify and exclude the few AGNs in the sample. To do so, we use a combination of the PRIMUS spectra, matching X-ray data, and IR colors of the galaxies.

As stated in Section 2.1, we only select objects classified as galaxies and did not include those classified as broad-line AGNs in the PRIMUS spectroscopy. For X-ray AGNs, we exclude galaxies with matched X-ray detections in the 4.3 deg^2 of X-ray coverage from *Chandra* and/or *XMM* telescopes (out of our full 6.7 deg^2). However, neither technique can exclude heavily-obscured AGNs effectively.

Finally, IR colors can be used to exclude strong AGNs. In the IRAC color-color diagram with $[3.6] - [4.5]$ versus $[5.8] - [8.0]$, AGNs occupy a different locus from normal galaxies, either SF or quiescent (Lacy et al. 2004; Stern et al. 2005). This is because the SED of an AGN in the IR can be well-represented by a power law, while that of a quiescent galaxy approximately follows Rayleigh-Jeans law and that of a SF galaxy is dominated by warm dust and PAH emission. To identify AGNs, we adopt the empirical criteria suggested by Stern et al. (2005). These criteria may omit AGNs at high redshift, but are adequate for our purpose since our sample is at $z < 0.5$. In Figure 3, we show the IRAC color-color diagram for all the detections in both the 5.8 and 8.0 channels in the flux-limited red-sequence sample, with Stern et al. (2005) criteria as the dotted wedge. Objects within the wedge are classified as AGNs (green filled squares). We also show SF and quiescent galaxies among the non-AGNs, defined in the next section, with blue filled triangles and red filled stars, respectively. The green dot-

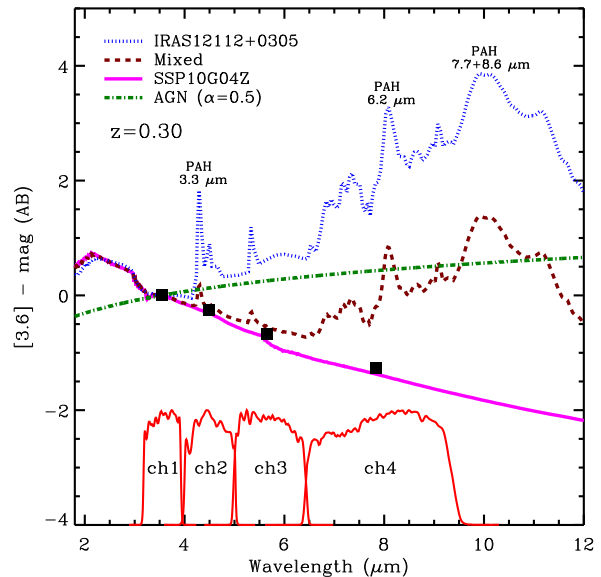


FIG. 5.— Spectral templates shifted to $z = 0.30$, in AB magnitudes, normalized to have the same magnitude zeropoint in the $3.6 \mu\text{m}$ channel. We use the template of IRAS12112 + 0305 from Rieke et al. (2009) to represent strong star-forming galaxies. For early-type galaxies without star formation and dust, we use a simple stellar population (SSP) with an age of 10 Gyr and metallicity of $0.4Z_{\odot}$ (SSP10G04Z) from the Bruzual & Charlot (2003) models. This template is approximately the average of a variety of SSPs with age ranging from 5 to 10 Gyr and metallicity of $0.4Z_{\odot}$ and $1.0Z_{\odot}$. We show the average magnitudes in IRAC channels of these SSPs in black filled squares. To classify star-forming and quiescent galaxies, we define a demarcation template (Mixed) by linearly combining the two templates. Normalized at $2 \mu\text{m}$, the Mixed template is the sum of 10% of IRAS12112 + 0305 and 90% of SSP10G04Z, and represents a galaxy with $\text{SSFR} \sim 10^{-10} \text{ yr}^{-1}$. The green dot-dashed line represents a power-law spectrum $f(\nu) = \nu^{-\alpha}$ of an AGN with $\alpha = 0.5$. We also show the response curves of IRAC channels on the bottom.

dashed line represents the colors of AGNs with power-law spectra $f(\nu) = \nu^{-\alpha}$, with α ranging from 0.5 to 3.0.

The Stern et al. (2005) method to identify AGNs requires detections in all four channels. In the flux-limited red-sequence sample, a large fraction (1288 of 3310) are not detected in the $8.0 \mu\text{m}$ channel. Nevertheless, we will show in the next section that we can safely classify them as quiescent galaxies. Among those (2022 of 3310) detected in the $8.0 \mu\text{m}$ channel, 154 do not have matched detections in the $5.8 \mu\text{m}$ channel due to the relatively bright flux limits. For these objects, we use the flux limits of $[5.8] < 19.8$ (21.3) mag in the SWIRE (S-COSMOS) fields to calculate the lower limits of their $[5.8] - [8.0]$ colors. We show the results in Figure 4. The colors of all $5.8 \mu\text{m}$ non-detections are unambiguously outside the AGN wedge and we therefore can safely classify them as non-AGNs and perform further SF and quiescent galaxy classification in the next section.

3.4. Classification of star-forming and quiescent galaxies

To separate SF and quiescent galaxies, we combine representative SED templates of strong SF galaxies and typical quiescent early-type galaxies. For strong SF galaxies, we choose the template of IRAS12112 + 0305

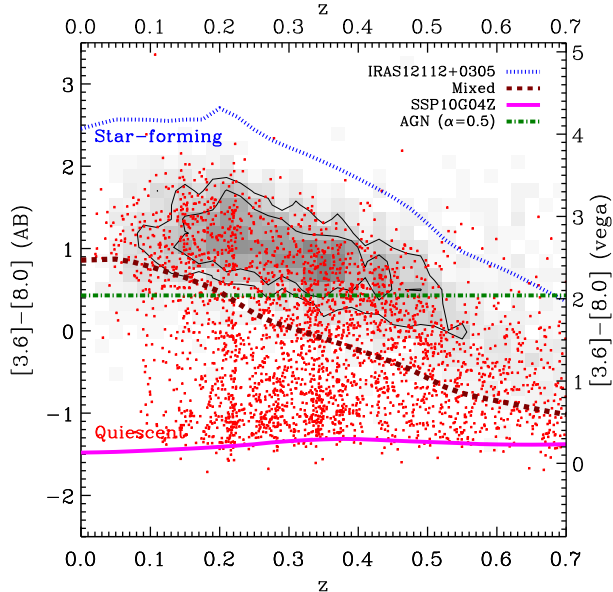


FIG. 6.— IR Color $[3.6] - [8.0]$ of the spectral templates in Figure 5, as a function of redshift. The various lines represent the colors of all the spectral templates in the same colors and line styles as in Figure 5. For comparison, we also show all the $8.0 \mu\text{m}$ detections in the blue-cloud (gray scale) and red-sequence galaxies (red dots) with $i < 22.5$ at $z < 0.7$. We classify galaxies above the Mixed template (the brown dashed line) as star-forming galaxies, if they are not in the AGN wedge in the IRAC color-color diagram (Figure 3). At $z > 0.5$, the $6.2 \mu\text{m}$ PAH feature shifts out of the $8.0 \mu\text{m}$ channel, causing the colors of star-forming and quiescent galaxies to blend into each other.

from Rieke et al. (2009), an ultra-luminous IR galaxy (ULIRG) with significant ongoing star formation (e.g., Armus et al. 2007). For typical quiescent early-type galaxies, we use a simple stellar population (SSP) with an age of 10 Gyr and metallicity of $0.4Z_{\odot}$ from the Bruzual & Charlot (2003) models, with the Padova 1994 library of stellar evolution tracks and the Chabrier (2003) Initial Mass Function (IMF). We denote this template as SSP10G04Z. In Figure 5, we show these templates, shifted to $z = 0.3$, within the wavelength range 2 to $12 \mu\text{m}$. We also show a power-law spectrum $f(\nu) = \nu^{-\alpha}$ with $\alpha = 0.5$ to represent a typical AGN. Note we have normalized all the SEDs to have the same magnitude zeropoint in the $3.6 \mu\text{m}$ channel for clarity. The IRAS12112 + 0305 template is dominated by warm dust continuum and strong PAH features. Meanwhile, the SSP template roughly follows the Rayleigh-Jeans law $f(\lambda) \propto \lambda^{-4}$. This template is similar to the average of a variety of SSPs with age ranging from 5 Gyr to 15 Gyr and metallicity of $0.4Z_{\odot}$ and $1.0Z_{\odot}$. We show the average magnitudes of these SSPs in the IRAC channels in black filled squares.

To define a demarcation template separating SF and quiescent galaxies, we linearly combine the templates of IRAS12112 + 0305 and SSP10G04Z. We first normalize them to have the same flux at $2 \mu\text{m}$ (roughly K -band), and then define the demarcation mixed template (Mixed hereafter) to be the sum of 10% of IRAS12112 + 0305 and 90% of SSP10G04Z. This Mixed template represents a galaxy with $\text{SSFR} \sim 10^{-10} \text{ yr}^{-1}$. We show the template

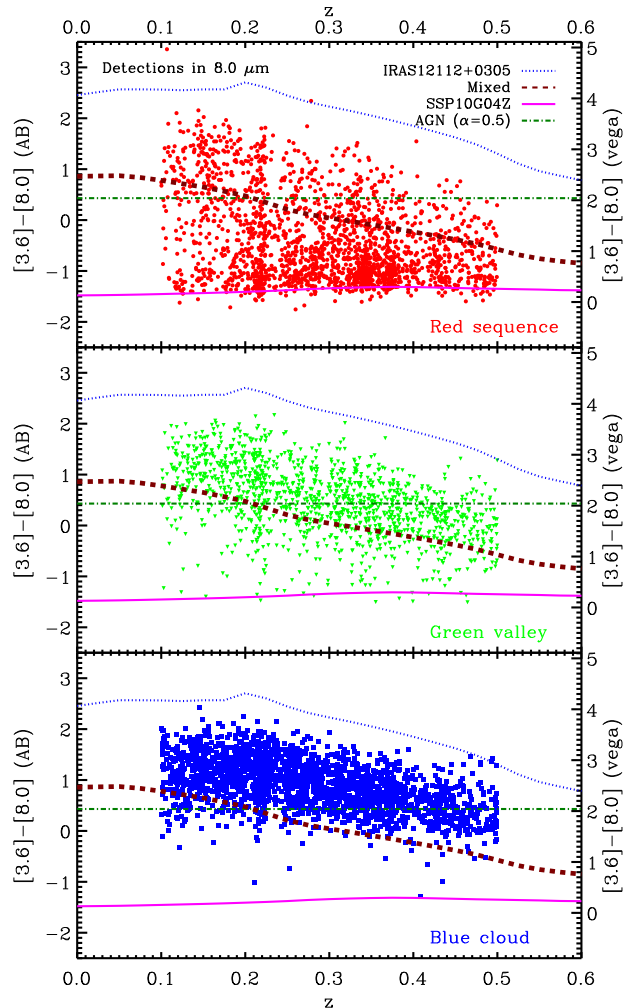


FIG. 7.— IR Color $[3.6] - [8.0]$ vs. z for all $8.0 \mu\text{m}$ detections in the flux-limited sample ($i < 20 \text{ mag}$ in the SWIRE fields and $i < 21 \text{ mag}$ in the S-COSMOS field). *Top panel:* red-sequence galaxies. Many are scattered into the star-forming region (above the Mixed template). *Middle panel:* green-valley galaxies. Most of them appear in the star-forming region. *Bottom panel:* blue-cloud galaxies. Almost all of them are in the star-forming region.

with the brown dashed line in Figure 5.

Figure 6 presents the $[3.6] - [8.0]$ colors of these templates as a function of redshift and compares them with those of the $8.0 \mu\text{m}$ detections among the red-sequence (red dots) and blue-cloud galaxies (gray scale) with $i < 22.5$ at $z < 0.7$. The IRAS12112 + 0305 template clearly defines the upper edge of the space of the blue-cloud galaxies. Meanwhile, the Mixed template follows the lower edge of the blue-cloud galaxies. Most of the red-sequence galaxies have redder colors than the typical SSP template, SSP10G04Z, which should not be surprising because very few galaxies are dust-free and can be accurately represented by SSPs. There are also many red-sequence galaxies scattered above the Mixed template, indicating they are in fact actively forming stars but their optical colors are reddened due to dust extinction. We also see that above $z = 0.5$, the colors of SF and quiescent galaxies start to blend into each other because the $6.2 \mu\text{m}$ PAH emission band shifts out of the

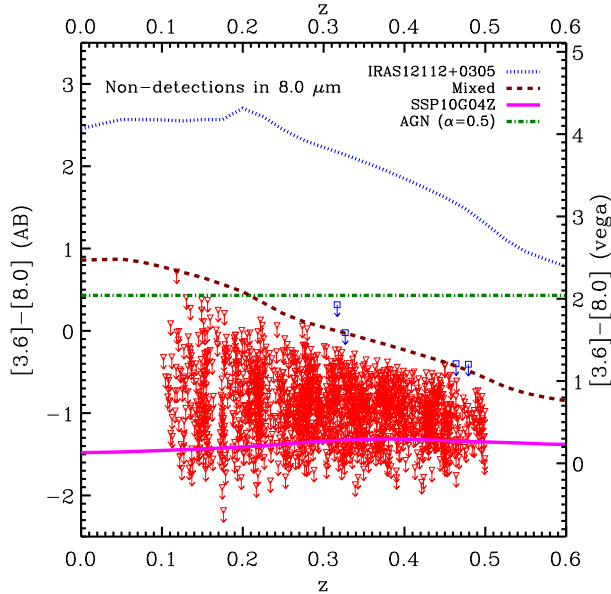


FIG. 8.— IR Color $[3.6] - [8.0]$ vs. z for non-detections in the $8.0 \mu\text{m}$ channel in the flux-limited red-sequence sample. We use the flux limits $[8.0] < 19.9$ (21.0) mag in the SWIRE (S-COSMOS) fields to calculate the upper limits of their $[3.6] - [8.0]$ colors. Almost all the non-detections fall below the demarcation line (the Mixed template). There are four galaxies that can be identified as star-forming galaxies if their $[8.0]$ fluxes are actually close to the flux limits. We treat them as quiescent galaxies, but identifying them as star-forming galaxies does not change our results.

$8.0 \mu\text{m}$ channel and we can not use the $[3.6] - [8.0]$ color to identify SF galaxies any more. Also there are very few galaxies below $z = 0.1$ because of the small volume in the observation cone. We therefore only focus our analysis on the redshift range $0.1 < z < 0.5$.

In Figure 7, we present the $[3.6] - [8.0]$ colors of all $8.0 \mu\text{m}$ detections in the flux-limited sample split by optical color. In the top panel, we show that a significant fraction of the red-sequence galaxies are scattered into the SF region. In the middle panel, we show that most of the green-valley galaxies are actually actively forming stars at roughly the same level as the blue-cloud galaxies. Therefore, that the green valley is redder than the blue cloud is likely not an indication of a much lower SSFR, but may be due to dust reddening. In the bottom panel, we show almost all of the blue-cloud galaxies appear in the SF region.

The classification of SF and quiescent galaxies requires detections in both the $3.6 \mu\text{m}$ and $8.0 \mu\text{m}$ channels. Among the 3310 red-sequence galaxies in the flux-limited sample, 1288 of them do not have matched $8.0 \mu\text{m}$ detections. For these galaxies, we use the flux limits of $[8.0] < 19.9$ (21.0) mag in the SWIRE (S-COSMOS) fields, to calculate the upper limits of their $[3.6] - [8.0]$ colors. We show the results in Figure 8. Only four of these objects may be identified as SF galaxies if their $[8.0]$ fluxes are close to the flux limits. Therefore the flux cuts in i band we adopt in Section 3.1 have provided a sample with bright $3.6 \mu\text{m}$ band fluxes (Figure 1) and enable us to reliably classify almost all of the $8.0 \mu\text{m}$ non-detections as quiescent galaxies. Below we treat the ambiguous four objects as quiescent galaxies

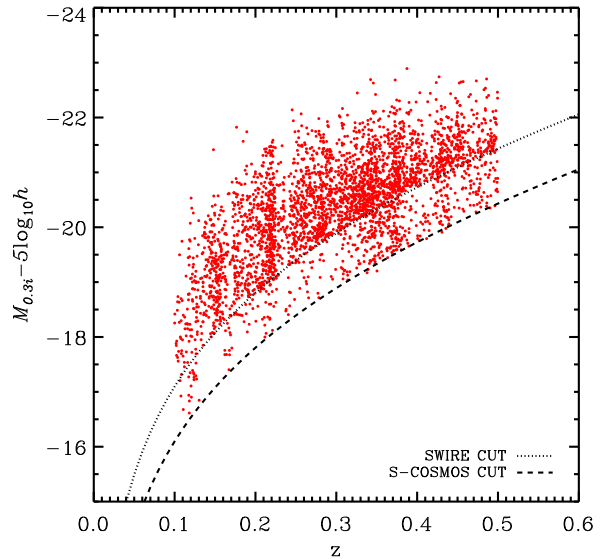


FIG. 9.— $M_{0.3i} - 5 \log_{10} h$ vs. z of the flux-limited red-sequence sample. The dotted line shows the flux cut $i = 20$ mag in the SWIRE fields and the dashed line represents the cut $i = 21$ mag in the S-COSMOS field, corrected with average K -corrections of red-sequence galaxies. Due to Malmquist bias, we are investigating higher luminosity at higher redshift.

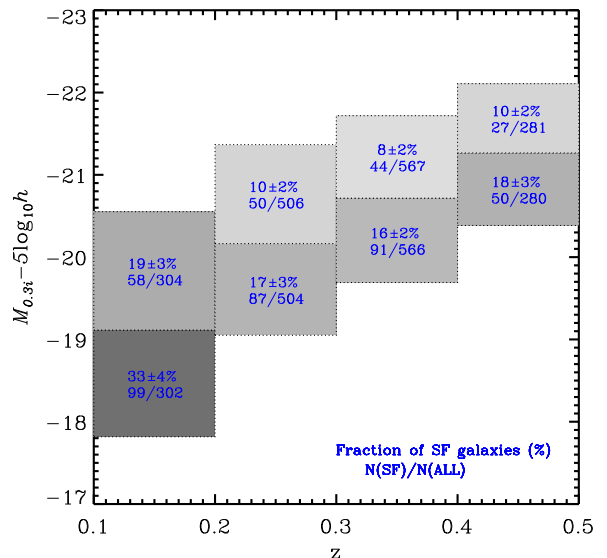


FIG. 10.— Fraction of obscured SF galaxies on the red sequence as a function of luminosity and redshift. In each redshift bin, we divide the sample into two subsamples with equal number of galaxies based on their luminosities and calculate the fraction of SF galaxies and Poisson errors. At all redshifts, the fraction is higher at lower luminosity. We visualize the fraction with gray scale (darker color represents higher fraction).

TABLE 1
FRACTION OF OBSCURED STAR-FORMING GALAXIES ON THE RED SEQUENCE

z	$\langle M_{0.3i} - 5 \log_{10} h \rangle$	$\langle M_{0.3i} - 5 \log_{10} h \rangle_{\text{cor}}^{\text{a}}$	N_{RS}^{b}	N_{SF}^{c}	Fraction of SF galaxies
$0.1 < z < 0.2$	-18.47	-18.64	302	99	$33 \pm 4\%$
$\langle z \rangle = 0.16$	-19.83	-20.01	304	58	$19 \pm 3\%$
$0.2 < z < 0.3$	-19.61	-19.67	504	87	$17 \pm 3\%$
$\langle z \rangle = 0.25$	-20.77	-20.83	506	50	$10 \pm 2\%$
$0.3 < z < 0.4$	-20.20	-20.15	566	91	$16 \pm 2\%$
$\langle z \rangle = 0.35$	-21.22	-21.16	567	44	$8 \pm 2\%$
$0.4 < z < 0.5$	-20.83	-20.65	280	50	$18 \pm 3\%$
$\langle z \rangle = 0.44$	-21.69	-21.52	281	27	$10 \pm 2\%$

^a $\langle M_{0.3i} - 5 \log_{10} h \rangle$ corrected to $z = 0.3$, assuming $dM_{0.3i}/dz = -1.2$ mag per unit redshift.

^b Number of red-sequence (RS) galaxies.

^c Number of star-forming (SF) galaxies in the red-sequence subsample.

as well. However, we emphasize that treating them as SF galaxies does not have any noticeable effect in our analysis. We present the results in the next section.

4. RESULTS: OBSCURED STAR FORMATION ON THE RED SEQUENCE

With the classification scheme of AGNs, SF galaxies, and quiescent galaxies defined in Section 3, we present a quantitative study of the fraction of obscured SF galaxies on the red sequence in this section.

4.1. Overall contribution

In total, we have 3310 red-sequence galaxies in the flux-limited sample at $0.1 < z < 0.5$. Among these we identify 15% (506) as SF galaxies, 84% (2783) as quiescent galaxies, and 1% (21) as AGNs. Note if we did not exclude X -ray detections in about two-thirds of the total 6.7 deg^2 fields, we would have 31 AGNs instead. In this flux-limited red-sequence sample, we find that overall 15% have IR colors consistent with star formation, indicating their optical colors are likely reddened due to dust extinction.

4.2. Luminosity dependence and redshift evolution

It is well-known that elliptical galaxies dominate the bright end of the red sequence while disk-dominated systems dominate the faint end (e.g., Marinoni et al. 1999; Bundy et al. 2010; Zhu et al. 2010). If the obscuration of the SF galaxies on the red sequence is due to high inclination, it is likely that the fraction of obscured SF galaxies also depends on luminosity. Additionally, the global star formation rate (SFR) has declined by roughly an order-of-magnitude since $z \sim 1$ (e.g., Madau et al. 1996; Hopkins et al. 2006; Zhu et al. 2009; Rujopakarn et al. 2010), therefore we may expect that the fraction of obscured SF galaxies on the red sequence has declined with decreasing redshift. We investigate the luminosity dependence and redshift evolution in this section.

For a flux-limited sample, due to Malmquist bias, the average luminosity is higher at higher redshift. We show this in Figure 9, where we plot the absolute magnitude $M_{0.3i} - 5 \log_{10} h$ versus z of the red-sequence galaxies. We also show the i band flux cuts, 20 mag in the SWIRE fields and 21 mag in the S-COSMOS field, corrected with average K -corrections of red-sequence galaxies, with the dotted and dashed lines, respectively.

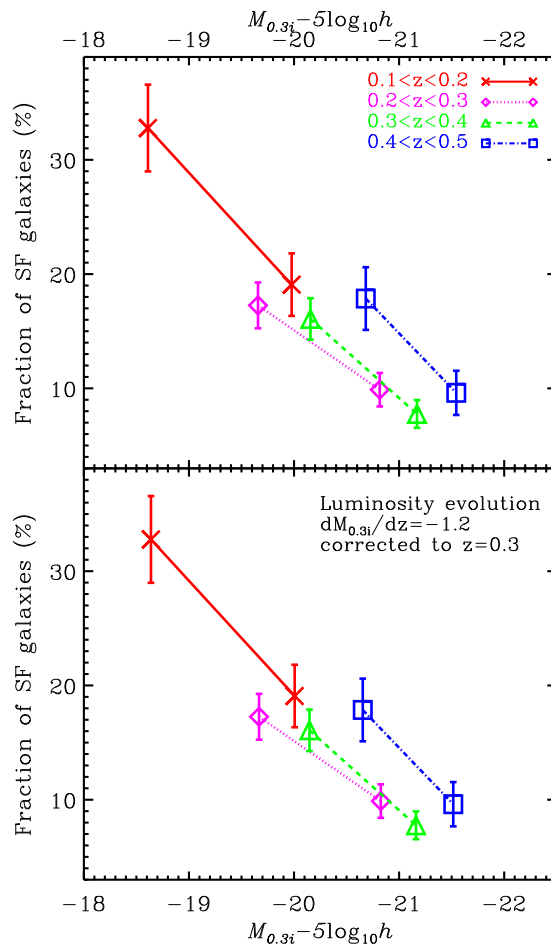


FIG. 11.— Fraction of obscured SF galaxies on the red sequence as a function of luminosity and redshift, as in Figure 10. We show the fraction at the mean magnitude in each subsample. In the bottom panel, we assume that $0.3i$ band absolute magnitude fades by 1.2 per unit redshift and correct all magnitudes to $z = 0.3$. In all redshift bins, the fraction (in percent) is higher at lower luminosity by $\sim 8\%$ per mag. Assuming linear luminosity dependence, at $L \gtrsim L^*$, the percentage of obscured SF galaxies has decreased by $\sim 6 \pm 3\%$ from $z = 0.44$ to $z = 0.25$. At $L \lesssim L^*$, the data from $z = 0.35$ to $z = 0.16$ are consistent with each other, within the errors. At fainter luminosity ($\gtrsim 1$ mag fainter than L^*), we do not have a wide enough redshift baseline to test for redshift evolution.

To overcome the Malmquist bias and possible degeneracy between luminosity and redshift dependence, we therefore define four redshift bins with a small binsize $\Delta z = 0.1$. In each redshift bin, we divide the sample into two subsamples with equal number of red-sequence galaxies based on their $M_{0.3i} - 5 \log_{10} h$ magnitudes.

Figure 10 presents the fraction of SF galaxies with Poisson errors at the mean absolute magnitude and redshift of each subsample. We visualize the fraction with gray scale (darker colors indicate higher fractions). We also list the results in Table 1. The fraction appears to be higher at lower luminosity in all four redshift bins.

We show the luminosity dependence in Figure 11, where we plot the fraction as a function of the mean $M_{0.3i} - 5 \log_{10} h$ in each subsample in the top panel. In the bottom panel, we assume that the luminosity fades with decreasing redshift by 1.2 mag per unit redshift, which is the luminosity evolution factor for an SSP with Salpeter (1955) IMF formed at $z \sim 4$ (e.g., van Dokkum 2008), and correct all luminosities to $z = 0.3$. We find that on average, at $0.1 < z < 0.5$, the fraction of SF galaxies on the red sequence is about 15% at $M_{0.3i} - 5 \log_{10} h \sim -20.5$ (about L^{*13}). And at all redshifts, the fraction (in percent) increases by $\sim 8\%$ per mag with decreasing luminosity to $0.2L^*$. For example, in the redshift range $0.3 < z < 0.4$, the fraction increases from $8 \pm 2\%$ to $16 \pm 2\%$ as luminosity decreases from $M_{0.3i} - 5 \log_{10} h \sim -21.2$ to -20.2 .

Also due to Malmquist bias, at different luminosities we are investigating different redshift ranges. Bundy et al. (2010) find that at stellar mass $\lesssim 10^{11} M_{\odot}$, the abundance of red-sequence disk galaxies increases with decreasing redshift, but not as fast as red-sequence spheroidals. They also find that at higher stellar mass, the disk population has declined since $z \sim 1$. If the obscured SF population behaves as their selected disk population, we expect that the redshift evolution of the fraction also depends on luminosity. With our flux-limited sample, each luminosity range covers a different redshift range, complicating our attempt to investigate this question. Figure 11 does not reveal any strong trend of evolution strength with luminosity, but we cannot address this question substantially below L^* with this sample. With our sample, assuming linear luminosity dependence, at $L \gtrsim L^*$ (e.g., at $M_{0.3i} - 5 \log_{10} h \sim -21$), the percentage of obscured SF galaxies on the red sequence has decreased by $\sim 6 \pm 3\%$ from $z = 0.44$ to $z = 0.25$. At $L \lesssim L^*$, the data from $z = 0.35$ to $z = 0.16$ are consistent with each other, within the errors. At fainter luminosity ($\gtrsim 1$ mag fainter than L^*), we do not have a wide enough redshift baseline to put interesting constraints on evolution.

4.3. The origin of 24 μm emission on the red sequence

We have shown that a significant fraction (15%) of red-sequence galaxies have IR colors consistent with star formation. Another approach to search for star formation is to use the 24 μm band of MIPS, also onboard *Spitzer*. The 24 μm emission is a close tracer of SFR of SF galaxies (e.g., Calzetti et al. 2007; Rieke et al. 2009). Previous studies (e.g., Davoodi et al. 2006; Rodighiero et al.

¹³ At $z \sim 0.1$, the L^* is $M_{0.1r} - 5 \log_{10} h \sim -20.4$ in $0.1r$ band (Blanton et al. 2003b) and $0.1r$ band is very close to $0.3i$ band.

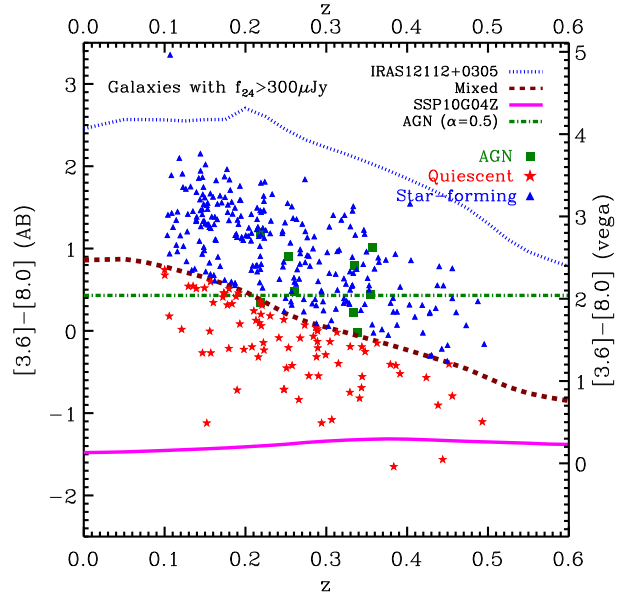


FIG. 12.— IR color $[3.6] - [8.0]$ vs. z for red-sequence galaxies with 24 μm emission $f_{24} > 300 \mu\text{Jy}$. We show star-forming galaxies in blue filled triangles, quiescent galaxies in red filled stars, and AGNs in green filled squares. At $0.1 < z < 0.5$, there are 355 ($\sim 11\%$ of the sample) galaxies with $f_{24} > 300 \mu\text{Jy}$, among which we identify $\sim 74\%$ (265) as SF galaxies, $\sim 23\%$ (81) as quiescent galaxies, and $\sim 3\%$ (9) as AGNs. The various lines represent spectral templates, as in Figure 5.

2007; Brand et al. 2009) find $\sim 10 - 20\%$ of red-sequence galaxies with 24 μm emission $f_{24} \gtrsim 300 \mu\text{Jy}$. With the 24 μm imaging data, we also find that in our flux-limited red-sequence sample at $0.1 < z < 0.5$, about 11% (355) have 24 μm flux $f_{24} > 300 \mu\text{Jy}$. At $z = 0.3$, this 24 μm flux corresponds to a SFR $\sim 3 M_{\odot}\text{yr}^{-1}$ (Rieke et al. 2009).

The 24 μm emission, however, can also originate from AGNs (e.g., Farrah et al. 2003; Brand et al. 2006). It is interesting to investigate whether star formation or AGN or both activities are responsible for the 24 μm emission of these red-sequence galaxies. Previous studies (e.g., Davoodi et al. 2006; Rodighiero et al. 2007; Brand et al. 2009) find that both star formation and AGN activities could be responsible. Brand et al. (2009) select 89 ($\sim 10\%$) red-sequence galaxies with $f_{24} > 300 \mu\text{Jy}$ from the AGN and Galaxy Evolution Survey (AGES) and employ both the emission-line diagnostic diagram (Baldwin et al. 1981, BPT) and the IRAC color-color diagram to investigate the origin of the emission. They find that in their sample, with the former method the majority ($\sim 64\%$) are identified as AGNs, while with the latter they identify $\sim 64\%$ as SF galaxies, $\sim 31\%$ as quiescent galaxies, and only $\sim 5\%$ as AGNs. Therefore both star formation and AGN activities take place in their sample, but in the optical the star formation is obscured by dust and in the IR the AGN emission is outshone by star formation emission.

The PRIMUS spectroscopy does not resolve the narrow lines required to construct the BPT diagram. However, we can perform the same AGN, SF galaxy, and quiescent galaxy classification as above using IRAC colors. Among

the 355 red-sequence galaxies with $f_{24} > 300 \mu\text{Jy}$, we identify $\sim 74\%$ (265) as SF galaxies, $\sim 23\%$ (81) as quiescent galaxies, and $\sim 3\%$ (9) as AGNs. In Figure 12, we plot the $[3.6] - [8.0]$ colors of these galaxies as a function of redshift. Our results are consistent with Brand et al. (2009) and suggest that star formation should account for at least part of the $24 \mu\text{m}$ emission.

5. DISCUSSION

5.1. The nature of galaxies on the red sequence

Although the red sequence is a well-defined locus with very small scatter in the color-magnitude diagram, it actually consists of both early-type and late-type galaxies: early-type spheroidal galaxies, late-type disk-dominated galaxies without ongoing star formation, and late-type dusty SF galaxies with their optical colors reddened due to dust extinction (e.g., edge-on Sb/Sc, etc.). When studying galaxy evolution based on optical color, it is therefore necessary to understand the contribution of different types of galaxies on the red sequence. Here we describe a number of methods of doing so, finding that broadly speaking they agree with our results here on the fraction of star-forming and/or disk galaxies on the red sequence.

There are many ways to study the composition of galaxies on the red sequence. A non-exhaustive list includes:

- (1) direct classification into different morphologies (e.g., Marinoni et al. 1999; Yan & Thompson 2003; Moustakas et al. 2004; Bell et al. 2004b; Weiner et al. 2005; Lotz et al. 2008; Blanton & Moustakas 2009; Bundy et al. 2010; Zhu et al. 2010);
- (2) using inclination-corrected properties (e.g., Tully et al. 1998; Masters et al. 2003; Shao et al. 2007; Driver et al. 2007; Bailin & Harris 2008a,b; Unterborn & Ryden 2008; Maller et al. 2009);
- (3) SED fitting where dust extinction is a free parameter (e.g., Kauffmann et al. 2003; Wolf et al. 2004; Brammer et al. 2009);
- (4) using optical color and optical-near-IR (NIR) color-color diagram (e.g., Pozzetti & Mannucci 2000; Labbé et al. 2005; Wuyts et al. 2007; Williams et al. 2009);
- (5) using IR color (e.g., Brand et al. 2009, this work);
- (6) using MIR flux (e.g., Coia et al. 2005; Davoodi et al. 2006; Rodighiero et al. 2007; Saintonge et al. 2008; Brand et al. 2009, this work);
- (7) using emission line measurements (e.g., Hammer et al. 1997; Demarco et al. 2005; Popesso et al. 2007; Verdugo et al. 2008).

It is difficult to carry out an exact comparison of these studies because of different sample selection methods, different luminosity and mass ranges investigated, and different redshift ranges investigated. However, all of these studies lead to the conclusion that a significant fraction of red-sequence galaxies are disk galaxies and/or obscured SF galaxies. Detailed studies conclude that the fraction depends strongly on luminosity and/or mass. In

terms of morphology, in the local universe, various papers (e.g., Marinoni et al. 1999; Zhu et al. 2010) have shown that spheroidal galaxies dominate the bright end ($\gtrsim L^*$) and disk-dominated systems dominate at the faint end. At redshifts $0.2 < z < 1.2$, Bundy et al. (2010) find that disk galaxies represent nearly one-half of all red-sequence population and dominate at low stellar mass $\lesssim 10^{10} M_\odot$. In terms of star formation, we find at redshifts $0.1 < z < 0.5$, the fraction of obscured SF galaxies on the red sequence increases by $\sim 8\%$ per mag with decreasing luminosity to $L \sim 0.2L^*$.

The redshift evolution of the relative fractions of different components on the red sequence, however, is less clear. Moustakas et al. (2004, see also Yan & Thompson 2003) find that the fraction of spheroidal galaxies in extremely red objects (EROs) is $33\% - 44\%$ at redshift $\sim 1 - 2$. Lotz et al. (2008) find that at luminosity brighter than $0.4L_B^*$, edge-on and dusty disk galaxies are almost one third of the red sequence at $z \sim 1.1$, while they only make up $\lesssim 10\%$ at $z \sim 0.3$. We also find that at $L \gtrsim L^*$, the fraction of obscured SF galaxies decreases by $\sim 6 \pm 3\%$ from $z = 0.44$ to $z = 0.25$. However, other studies do not find a noticeable redshift dependence. Bell et al. (2004b) and Weiner et al. (2005) find that the fraction of edge-on disk galaxies is similar at $z \sim 1$ and at $z \sim 0$. One possible reason for the disagreement is that the redshift evolution of relative fractions may depend on other properties such as stellar mass or luminosity. For example, Bundy et al. (2010) find that at stellar mass $\lesssim 10^{11} M_\odot$, the abundance of red-sequence disk galaxies increases with decreasing redshift, but not as fast as red-sequence spheroidals; meanwhile, at higher stellar mass, the disk population has declined since $z \sim 1$.

The relative fractions of different types of galaxies and their redshift evolution on the red sequence may also depend on environment. It is well-known that overall early-type galaxies are more frequently found in high-density environments while late-type galaxies tend to dominate in low-density regions (the Morphology-density relation, Dressler 1980). There is also the SSFR-density relation such that the mean SSFR is higher at low density, an effect that is important in the local universe as well as at $z \sim 1$ (e.g., Kauffmann et al. 2004; Cooper et al. 2008). Meanwhile, the mean SFR is higher at low density in the local universe but the SFR-density relation appears to be reversed at $z \sim 1$ (e.g., Elbaz et al. 2007; Cooper et al. 2008). The fraction of obscured SF galaxies therefore may also depend on environment (e.g., Wolf et al. 2005; Gallazzi et al. 2008; Wolf et al. 2009; Feruglio et al. 2010). These studies suggest that in interpreting the optical color-magnitude diagram as a function of environment, the population of obscured SF galaxies may need to be accounted for.

An interesting suggestion by some papers is that the obscured SF galaxies on the red sequence are a third type other than red and blue galaxies (e.g., Wolf et al. 2005; Weinmann et al. 2006; Popesso et al. 2007; Bailin & Harris 2008a; Verdugo et al. 2008; Wolf et al. 2009). For example, Wolf et al. (2005) and Wolf et al. (2009) find these galaxies are distributed differently in environment than both the red and the blue galaxy populations: unlike red galaxies they tend to avoid dense cluster regions, but in contrast to blue

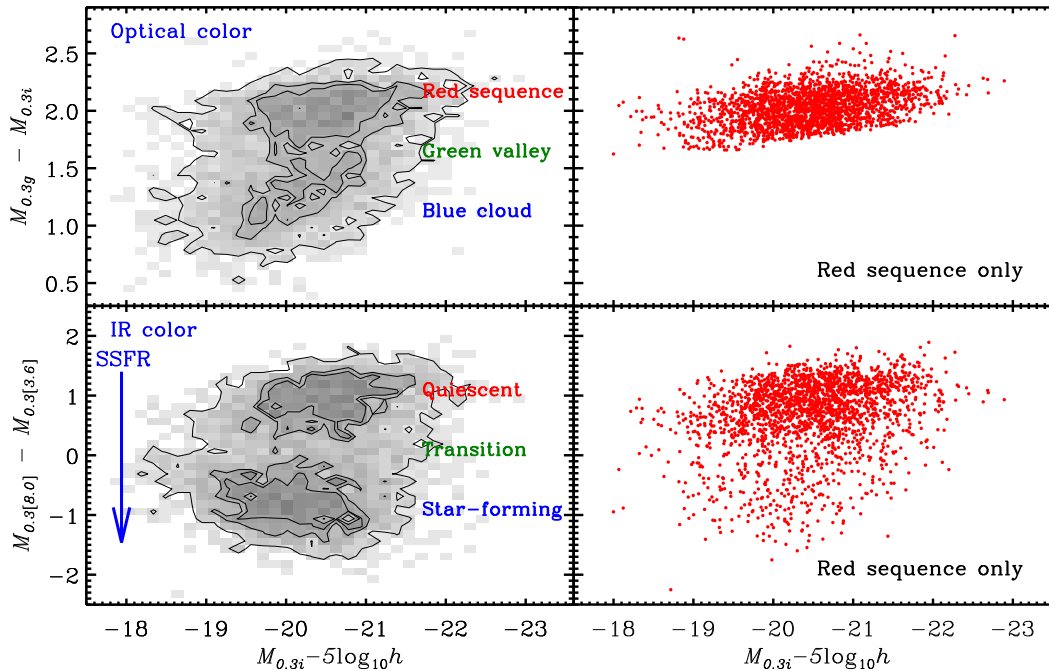


FIG. 13.— Color-magnitude diagram for galaxies between $z = 0.2$ and $z = 0.4$ in the flux-limited sample. *Upper-left panel*: Optical color $M_{0.3g} - M_{0.3i}$ vs. $M_{0.3i} - 5 \log_{10} h$. *Upper-right panel*: Optical color $M_{0.3g} - M_{0.3i}$ vs. $M_{0.3i} - 5 \log_{10} h$, but only for red-sequence galaxies. *Lower-left panel*: IR color $M_{0.3[8.0]} - M_{0.3[3.6]}$ vs. $M_{0.3i} - 5 \log_{10} h$. *Lower-right panel*: IR color $M_{0.3[8.0]} - M_{0.3[3.6]}$ vs. $M_{0.3i} - 5 \log_{10} h$, but only for red-sequence galaxies. The bimodality is more striking using IR color. And a significant fraction of red-sequence galaxies are scattered into the star-forming region in the IR color-magnitude diagram.

galaxies they are not common in low-density fields. With $24 \mu\text{m}$ MIR data, Wolf et al. (2009) further show that the mean SSFR of these galaxies in clusters is lower than in the field, in contrast to that of blue galaxies alone, which appears similar in different environments. They also show using *HST* imaging that edge-on spirals form only a small fraction of spiral galaxies. These authors thus suggest that these obscured SF galaxies are a transitioning population between blue field galaxies and red cluster galaxies in cores.

Finally, an interesting question is how much these obscured SF galaxies account for in the overall SFR density in the universe (e.g., Bell et al. 2007). In the flux-limited sample, we have 506 obscured SF galaxies on the red sequence, 1451 green-valley and 2497 blue-cloud galaxies. Assuming that they have comparable average SSFR and stellar mass, we roughly estimate that of order 10% of total cosmic star formation is contributed by obscured SF galaxies. An exact analysis requires precise SFR measurements, beyond the scope of this paper. We will address this issue in future papers measuring the global SFR density using UV and $24 \mu\text{m}$ MIR luminosity.

5.2. IR color-magnitude diagram

As a proxy for the SSFR-stellar mass relation, the optical color-magnitude diagram is a powerful tool in studying galaxy evolution; however, we argue here that IR color can be more effective in separating star-forming and quiescent galaxies when it is available. As shown above, optical color can be a misleading variable for SSFR and there is a significant fraction of obscured SF galaxies on

the red sequence. The fraction depends on luminosity and redshift and may also depend on environment. This complication affects galaxy evolution studies based on optical color. Therefore, it is useful to find more suitable variables tracing SSFR. Examples of such variables are inclination-corrected color (e.g., Maller et al. 2009) and extinction-corrected color from SED fitting (e.g., Brammer et al. 2009). IR color is another, and better, variable than optical color to represent SSFR; therefore, replacing optical color with IR color when available is a better strategy when constructing the color-magnitude diagram.

As an example, in Figure 13 we show both the optical color-magnitude diagram (*upper-left panel*) and IR color-magnitude diagram (*lower-left panel*), where we have reversed the IR color $[3.6] - [8.0]$ to $[8.0] - [3.6]$ so that SF galaxies are on the bottom. We show all the galaxies in the flux-limited sample at $0.2 < z < 0.4$. For non-detections in $8.0 \mu\text{m}$ channel, we use the lower limits by applying the flux limits $[8.0] < 19.9$ (21.0) mag in the SWIRE (S-COSMOS) fields. We have also applied simple K -corrections using the templates for IRAS12112 + 0305 and SSP10G04Z to correct the IR color $[8.0] - [3.6]$ so that it is the color in the channels shifted blueward to $z = 0.3$, i.e., $M_{0.3[8.0]} - M_{0.3[3.6]}$. The bimodality in the IR color-magnitude diagram is more striking than in the optical color-magnitude diagram. This should not be surprising because the bimodality is caused by the short time-scale of transition from star formation to quiescence. In the right panels, we only plot the red-sequence galaxies and show that a

significant fraction of them are in the SF region in the IR color-magnitude diagram, as we quantified in detail above.

6. SUMMARY

With the recently completed PRIMUS Multi-object Survey (PRIMUS), we perform a quantitative study of the fraction of obscured star-forming galaxies on the red sequence at intermediate redshift. PRIMUS targeted fields with existing deep infrared (IR) imaging from the IRAC and MIPS instruments onboard the *Spitzer Space Telescope*, including 5.7 deg² fields from the SWIRE survey and a 1 deg² field from the S-COSMOS survey. With the precise redshifts from PRIMUS, we select in these fields an *i* band flux-limited sample of 3310 red-sequence galaxies, with $i < 20$ mag in the SWIRE fields and $i < 21$ mag in the S-COSMOS field, at $0.1 < z < 0.5$. With the IR imaging data, we classify the red-sequence galaxies into AGNs, star-forming galaxies, and quiescent galaxies. Our sample is the largest sample at intermediate redshift for such a study and we present for the first time a quantitative analysis of the fraction of obscured star-forming galaxies on the red sequence as a function of luminosity.

We find that on average, at $L \sim L^*$, about 15% of red-sequence galaxies have IR colors ($[3.6] - [8.0]$) consistent with star-forming galaxies at $0.1 < z < 0.5$. The percentage of obscured star-forming galaxies increases by $\sim 8\%$ per mag with decreasing luminosity to $L \sim 0.2L^*$. At $L \gtrsim L^*$, the fraction has declined by $\sim 6 \pm 3\%$ from $z = 0.44$ to $z = 0.25$. At $L \lesssim L^*$, the fraction is consistent with no redshift evolution between $z = 0.35$ and $z = 0.16$.

Using the 24 μm imaging from MIPS on board *Spitzer*, we find that $\sim 11\%$ of red-sequence galaxies exhibit 24 μm emission with $f_{24} > 300 \mu\text{Jy}$ at redshifts $0.1 <$

$z < 0.5$, in agreement with previous studies. With the IRAC imaging, we find that $\sim 74\%$ of these galaxies have IR colors consistent with star-forming galaxies, suggesting that star formation accounts for at least part of the 24 μm emission.

Our analysis suggests that a significant fraction of red-sequence galaxies are actually actively forming stars, but their optical colors are reddened due to dust extinction. An accurate understanding of galaxy evolution using optical color therefore needs to account for this complication. We suggest that IR color, e.g., the IRAC color $[3.6] - [8.0]$, should be a better color to use when constructing the color-magnitude diagram to represent the specific star-formation rate-stellar mass relation.

We acknowledge Rebecca Bernstein, Adam Bolton, Douglas Finkbeiner, David W. Hogg, Timothy McKay, Sam Roweis, and Wiphu Rujopakarn for their contributions to the PRIMUS project. This paper includes data gathered with the 6.5 meter Magellan Telescopes located at Las Campanas Observatory, Chile. We thank the support staff at LCO for their help during our observations, and we acknowledge the use of community access through NOAO observing time. Funding for PRIMUS has been provided by NSF grants AST-0607701, 0908246, 0908442, 0908354 and NASA grant 08-ADP08-0019. RJC is supported by NASA through Hubble Fellowship grant HF-01217 awarded by the Space Telescope Science Institute, which is operated by the Association of Universities for Research in Astronomy, Inc., for NASA, under contract NAS 5-26555.

This work is based in part on observations made with the *Spitzer Space Telescope*, which is operated by the Jet Propulsion Laboratory (JPL), California Institute of Technology under a contract with NASA. We would like to thank the SWIRE and the S-COSMOS teams for making their data publicly available.

REFERENCES

- Armus, L., et al. 2007, ApJ, 656, 148
 Bailin, J., & Harris, W. E. 2008a, MNRAS, 385, 1835
 —. 2008b, ApJ, 681, 225
 Baldry, I. K., Glazebrook, K., Brinkmann, J., Ivezić, Ž., Lupton, R. H., Nichol, R. C., & Szalay, A. S. 2004, ApJ, 600, 681
 Baldwin, J. A., Phillips, M. M., & Terlevich, R. 1981, PASP, 93, 5
 Balogh, M. L., Baldry, I. K., Nichol, R., Miller, C., Bower, R., & Glazebrook, K. 2004, ApJ, 615, L101
 Bell, E. F., Phleps, S., Somerville, R. S., Wolf, C., Borch, A., & Meisenheimer, K. 2006a, ApJ, 652, 270
 Bell, E. F., Zheng, X. Z., Papovich, C., Borch, A., Wolf, C., & Meisenheimer, K. 2007, ApJ, 663, 834
 Bell, E. F., et al. 2004a, ApJ, 600, L11
 —. 2004b, ApJ, 608, 752
 —. 2006b, ApJ, 640, 241
 Blanton, M. R., & Moustakas, J. 2009, ARA&A, 47, 159
 Blanton, M. R., & Roweis, S. 2007, AJ, 133, 734
 Blanton, M. R., et al. 2003a, ApJ, 594, 186
 —. 2003b, ApJ, 592, 819
 Brammer, G. B., et al. 2009, ApJ, 706, L173
 Brand, K., et al. 2006, ApJ, 644, 143
 —. 2009, ApJ, 693, 340
 Brown, M. J. I., Dey, A., Jannuzi, B. T., Brand, K., Benson, A. J., Brodwin, M., Croton, D. J., & Eisenhardt, P. R. 2007, ApJ, 654, 858
 Bruzual, G., & Charlot, S. 2003, MNRAS, 344, 1000
 Bundy, K., et al. 2010, ApJ, 719, 1969
 Calzetti, D., et al. 2007, ApJ, 666, 870
 Chabrier, G. 2003, PASP, 115, 763
 Cimatti, A., Daddi, E., & Renzini, A. 2006, A&A, 453, L29
 Coia, D., et al. 2005, A&A, 430, 59
 Colless, M., et al. 2001, MNRAS, 328, 1039
 Coil, A. L., et al. 2010, ApJ, submitted
 Cool, R. J., et al. 2008, ApJ, 682, 919
 Cooper, M. C., et al. 2008, MNRAS, 383, 1058
 Davis, M., Huchra, J., Latham, D. W., & Tonry, J. 1982, ApJ, 253, 423
 Davis, M., et al. 2003, in Presented at the Society of Photo-Optical Instrumentation Engineers (SPIE) Conference, Vol. 4834, Society of Photo-Optical Instrumentation Engineers (SPIE) Conference Series, ed. P. Guhathakurta, 161–172
 Davoodi, P., et al. 2006, MNRAS, 371, 1113
 Demarco, R., et al. 2005, A&A, 432, 381
 Dressler, A. 1980, ApJ, 236, 351
 Driver, S. P., Popescu, C. C., Tuffs, R. J., Liske, J., Graham, A. W., Allen, P. D., & de Propriis, R. 2007, MNRAS, 379, 1022
 Eisenhardt, P. R., et al. 2004, ApJS, 154, 48
 Elbaz, D., et al. 2007, A&A, 468, 33
 Faber, S. M., et al. 2007, ApJ, 665, 265
 Farrah, D., Afonso, J., Efstathiou, A., Rowan-Robinson, M., Fox, M., & Clements, D. 2003, MNRAS, 343, 585
 Fazio, G. G., et al. 2004, ApJS, 154, 10
 Feruglio, C., et al. 2010, ApJ, 721, 607
 Gallazzi, A., Brinchmann, J., Charlot, S., & White, S. D. M. 2008, MNRAS, 383, 1439
 Garilli, B., et al. 2008, A&A, 486, 683
 Hammer, F., et al. 1997, ApJ, 481, 49

- Hopkins, P. F., Hernquist, L., Cox, T. J., Di Matteo, T., Robertson, B., & Springel, V. 2006, *ApJS*, 163, 1
- Kauffmann, G., White, S. D. M., Heckman, T. M., Ménard, B., Brinchmann, J., Charlot, S., Tremonti, C., & Brinkmann, J. 2004, *MNRAS*, 353, 713
- Kauffmann, G., et al. 2003, *MNRAS*, 341, 33
- Labbé, I., et al. 2005, *ApJ*, 624, L81
- Lacy, M., et al. 2004, *ApJS*, 154, 166
- Li, A., & Draine, B. T. 2001, *ApJ*, 554, 778
- Lilly, S. J., et al. 2007, *ApJS*, 172, 70
- Lonsdale, C. J., et al. 2003, *PASP*, 115, 897
- Lotz, J. M., et al. 2008, *ApJ*, 672, 177
- Madau, P., Ferguson, H. C., Dickinson, M. E., Giavalisco, M., Steidel, C. C., & Fruchter, A. 1996, *MNRAS*, 283, 1388
- Maller, A. H., Berlind, A. A., Blanton, M. R., & Hogg, D. W. 2009, *ApJ*, 691, 394
- Marinoni, C., Monaco, P., Giuricin, G., & Costantini, B. 1999, *ApJ*, 521, 50
- Martin, D. C., et al. 2005, *ApJ*, 619, L1
- Masters, K. L., Giovanelli, R., & Haynes, M. P. 2003, *AJ*, 126, 158
- Moustakas, L. A., et al. 2004, *ApJ*, 600, L131
- Popesso, P., Biviano, A., Romaniello, M., & Böhringer, H. 2007, *A&A*, 461, 411
- Pozzetti, L., & Mannucci, F. 2000, *MNRAS*, 317, L17
- Rieke, G. H., Alonso-Herrero, A., Weiner, B. J., Pérez-González, P. G., Blaylock, M., Donley, J. L., & Marcillac, D. 2009, *ApJ*, 692, 556
- Rieke, G. H., et al. 2004, *ApJS*, 154, 25
- Rix, H., et al. 2004, *ApJS*, 152, 163
- Rodighiero, G., Cimatti, A., Franceschini, A., Brusa, M., Fritz, J., & Bolzonella, M. 2007, *A&A*, 470, 21
- Rujopakarn, W., et al. 2010, *ApJ*, 718, 1171
- Saintonge, A., Tran, K., & Holden, B. P. 2008, *ApJ*, 685, L113
- Salpeter, E. E. 1955, *ApJ*, 121, 161
- Sanders, D. B., et al. 2007, *ApJS*, 172, 86
- Shao, Z., Xiao, Q., Shen, S., Mo, H. J., Xia, X., & Deng, Z. 2007, *ApJ*, 659, 1159
- Smith, J. D. T., et al. 2007, *ApJ*, 656, 770
- Stern, D., et al. 2005, *ApJ*, 631, 163
- Strateva, I., et al. 2001, *AJ*, 122, 1861
- Tully, R. B., Pierce, M. J., Huang, J., Saunders, W., Verheijen, M. A. W., & Witchalls, P. L. 1998, *AJ*, 115, 2264
- Untertorn, C. T., & Ryden, B. S. 2008, *ApJ*, 687, 976
- van Dokkum, P. G. 2008, *ApJ*, 674, 29
- Verdugo, M., Ziegler, B. L., & Gerken, B. 2008, *A&A*, 486, 9
- Weiner, B. J., et al. 2005, *ApJ*, 620, 595
- Weinmann, S. M., van den Bosch, F. C., Yang, X., & Mo, H. J. 2006, *MNRAS*, 366, 2
- Werner, M. W., et al. 2004, *ApJS*, 154, 1
- Williams, R. J., Quadri, R. F., Franx, M., van Dokkum, P., & Labbé, I. 2009, *ApJ*, 691, 1879
- Willmer, C. N. A., et al. 2006, *ApJ*, 647, 853
- Wolf, C., Gray, M. E., & Meisenheimer, K. 2005, *A&A*, 443, 435
- Wolf, C., Meisenheimer, K., Rix, H., Borch, A., Dye, S., & Kleinheinrich, M. 2003, *A&A*, 401, 73
- Wolf, C., et al. 2004, *A&A*, 421, 913
- . 2009, *MNRAS*, 393, 1302
- Wuyts, S., et al. 2007, *ApJ*, 655, 51
- Yan, L., & Thompson, D. 2003, *ApJ*, 586, 765
- York, D. G., et al. 2000, *AJ*, 120, 1579
- Zhu, G., Blanton, M. R., & Moustakas, J. 2010, *ApJ*, 722, 491
- Zhu, G., Moustakas, J., & Blanton, M. R. 2009, *ApJ*, 701, 86